



Combinatorial study of WInZnO films deposited by rf magnetron co-sputtering

Byeong-Yun Oh^a, Jae-Cheol Park^a, Young-Jun Lee^{a,b}, Sang-Jun Cha^c, Joo-Hyung Kim^b, Kwang-Young Kim^a, Tae-Won Kim^a, Gi-Seok Heo^{a,*}

^a National Center for Nanoprocess and Equipments, Korea Institute of Industrial Technology (KITECH), 110-9 Oryong-dong, Buk-gu, Gwangju 500-480, Republic of Korea

^b Department of Electronic Engineering, Chosun University, 375 Seoseok-dong, Dong-gu, Gwangju 501-759, Republic of Korea

^c Department of Physics, Chonnam National University, 300 Yongbong-dong, Buk-gu, Gwangju 500-757, Republic of Korea

ARTICLE INFO

Article history:

Received 13 May 2011

Received in revised form

12 July 2011

Accepted 14 July 2011

Available online 22 July 2011

Keywords:

Tungsten indium zinc oxide (WInZnO) films

Indium zinc oxide (IZO) films

Tungsten trioxide (WO₃)

Combinatorial rf magnetron co-sputtering

Compositionally spread films

Active channel layer

ABSTRACT

The compositional dependence of co-sputtered tungsten indium zinc oxide (WInZnO) film properties was first investigated by means of a combinatorial technique. Indium zinc oxide (IZO) and WO₃ targets were used with different target power. W composition ratio [W/(In+Zn+W)] was varied between 3 and 30 at% and film thickness was reduced as the sample position moved toward WO₃ target. Furthermore, the optical bandgap energy increased gradually, which might be affected by the reduction in film thickness. All the WInZnO films showed an amorphous phase regardless of the W/(In+Zn+W) ratio. As the W/(In+Zn+W) ratio in WInZnO films increased, the carrier concentration was restricted, causing the increase in electrical resistivity. W cations worked as oxygen binders in determining the electronic properties, resulting in suppressing the formation of oxygen vacancies. Consequentially, W metal cations were effectively incorporated into the WInZnO films as a suppressor against the oxygen vacancies and the carrier generation by employing the combinatorial technique.

© 2011 Elsevier Inc. All rights reserved.

1. Introduction

Recently, Zn-based amorphous oxide semiconductors (AOSs) have attracted considerable attention as promising candidates for driving thin-film transistors (TFTs) of future displays such as active-matrix organic light-emitting diodes (AMOLEDs) due to their low-temperature processing, potentially better device performance, and stability comparable to amorphous silicon TFT counterparts [1–3]. The composition of AOSs as an active channel layers such as In–Ga–Zn–O, In–Zn–O, Zn–In–Sn–O, Zn–Sn–O, and In–Al–Zn–O has been usually fabricated by mixing several metal oxides to improve the TFT device performance [3–7]. The group III and IV elements (e.g., Ga, Y, Si, Sn, Ti, Zr, and Hf) are considered to play important roles in suppressing charge carrier generation ($< \sim 10^{18} \text{ cm}^{-3}$) and in improving the stability of TFTs by binding with oxygen [3,4,8–12]. The elements composed of heavy-metal cations with $(n-1)d^{10}ns^0$ ($n \geq 4$) electronic configurations, especially In and Zn, can present the high electron mobility and stability due to ns^0 ($n \geq 4$) orbital overlap between adjacent orbitals [11,13]. Furthermore, most of the research has focused on the process parameters, semiconductor deposition methods, thermal annealing conditions, and electrical analyses.

In this study, we first report on a combinatorial investigation of tungsten trioxide (WO₃) as an oxygen binder in tungsten-indium-zinc oxide (WInZnO) semiconductor materials. The combinatorial radio-frequency (rf) magnetron co-sputtering geometry used is possible to make a compositionally spread film at once, thereby, the effect of W element on electrical properties of WInZnO films could be systematically studied. The electrical resistivity was rapidly affected by suppressing the charge carrier generation at W/(In+Zn+W) ratio of > 15.1 at% in WInZnO thin films.

2. Experimental

2.1. Film synthesis

WInZnO thin films were prepared on a glass substrate (180 × 50 mm) by a combinatorial rf magnetron co-sputtering system at room temperature (R.T) using a 10 wt% ZnO-doped In₂O₃ target (IZO, 4 N) and a WO₃ target (4 N). Fig. 1a shows the schematic diagram of the combinatorial sputtering, which consists of a vacuum chamber reactor (ULVAC MB07-4501) equipped with 4-in. sputtering guns at both sides of the substrate. The substrate with a shadow mask was located at a distance of 150 mm away from the targets. The sputtering chamber was initially evacuated to a base pressure of $< 5 \times 10^{-6}$ Pa and the

* Corresponding author.

E-mail address: gsheo@kitech.re.kr (G.-S. Heo).

working pressure for film deposition was maintained at 0.17 Pa using Ar (24.8 sccm) and O₂ (0.2 sccm) ambient gasses. Sputtering was carried out for 30 m with the IZO rf power of 200 W and the WO₃ rf power of 100 W. The substrate holder was not rotated during the sputtering. As a result, WInZnO film was compositionally graded by rf power for each target across the glass substrate as shown in Fig. 1b.

2.2. Characterization techniques

The composition of the films was examined by energy dispersive X-ray spectroscopy (EDS) and the result was summarized in Table 1. The surface roughness was analyzed by atomic force microscopy (AFM, XE-200 system). The film thickness was observed by a cross-sectional view of field emission scanning electron microscope (FE-SEM, Quanta 200). Optical transmission spectra were measured using a UV-vis-NIR spectrometer in the wavelength range (Varian Cary 5000). Sheet resistance was measured using a conventional four-point probe system (RT-3000/RG-100) and the electrical resistivity, free carrier

concentration, and Hall mobility were determined from the Hall effect measurements using the Van der Pauw geometry (Model 7707, LakeShore Cryotronics) at a constant magnetic field of 0.4 T. The crystal structure was characterized by X-ray diffraction (XRD) using monochromatic CuK α radiation with a wavelength of 1.5406 Å (X'Pert—PRO MRD XL).

3. Results and discussion

Fig. 2 shows the composition mapping in the ternary composition triangle, where each point represents the cation composition extracted from each sample. W content of WInZnO film increased as the sample position became close to W target, which was in contrast with In content. On the other hand, Zn content experienced little change. It was also found that O content of the films increased constantly from 69.5 to 91.1 at% as shown in Table 1. Namely, the amount of O element in WInZnO film increased with increasing W incorporation. As discussed below, it is therefore assumed that the W⁶⁺ ions works as oxygen binders in determining the electronic properties due to its high electronegativity ($W=2.4$), thereby possibly suppressing the formation of oxygen vacancies [10].

Fig. 3 shows the film thickness with respect to the sample position of WInZnO films and the sheet resistance (R_s), which was compositionally graded by rf power for each target. The R_s value had a tendency to increase consistently from 39.0 Ω /sq to 14.9 M Ω /sq as the sample position became close to W target, while the film thickness declined due to different rf power of each target and the target-to-substrate distance [14].

Fig. 4 shows the change in average transmittance of WInZnO films extracted in the wavelength range of 400–800 nm. Transmittance value increased consistently and then it decreased reversely. Although the transmittance is generally dependent on the film thickness, the resultant transmittance revealed the parabolic curve. This result implies that the contribution of W to optical property of WInZnO film is larger than the dependence

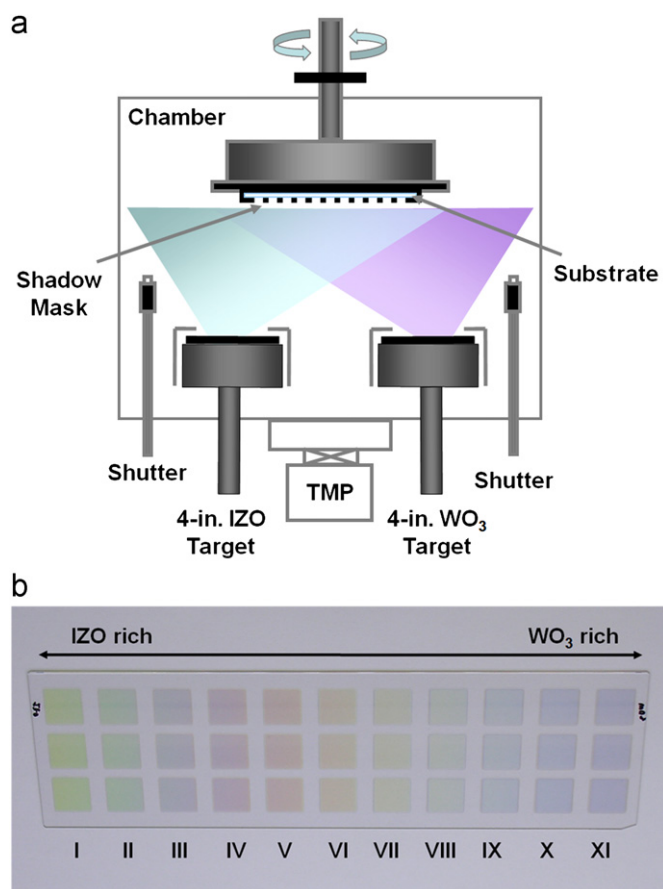


Fig. 1. (a) A schematic diagram of the combinatorial rf magnetron sputtering system for the deposition of WInZnO films and (b) the samples at various positions in the combinatorial library.

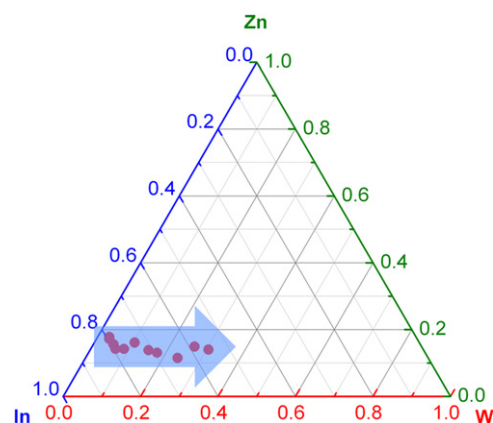


Fig. 2. Composition mapping in the ternary composition triangle. Each point represents the cation composition of WInZnO films.

Table 1

Chemical composition and $W/(In+Zn+W)$ ratio of the compositionally spread WInZnO films deposited by combinatorial rf magnetron co-sputtering system.

Sample position	I	II	III	IV	V	VI	VII	VIII	IX	X	XI
OK	69.5	71.8	74.2	77.8	79.9	81.1	84.7	87.3	89.1	89.5	91.1
InL	24.2	22.4	20.4	17.7	15.5	13.9	10.9	8.8	7.0	6.1	4.9
ZnK	5.4	4.8	4.0	3.1	2.9	3.0	2.1	1.7	1.3	1.6	1.3
WL	0.9	1.0	1.4	1.4	1.7	2.0	2.3	2.2	2.6	2.8	2.7
$W/(In+Zn+W)$ (at%)	3.0	3.3	5.2	6.4	8.6	10.4	15.1	17.7	23.8	26.5	30.5

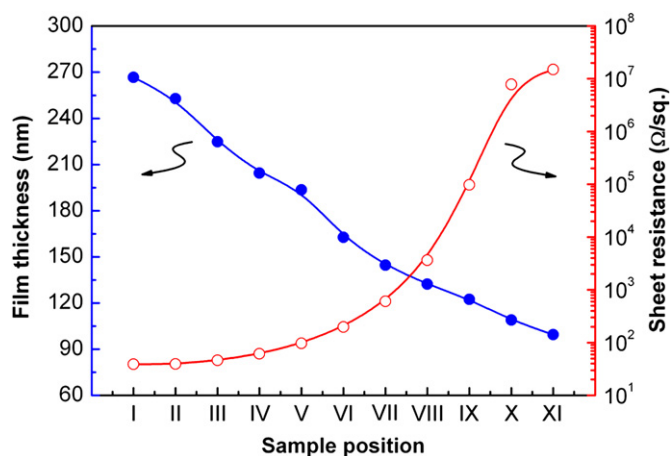


Fig. 3. Film thickness and sheet resistance of WInZnO films as a function of the sample position.

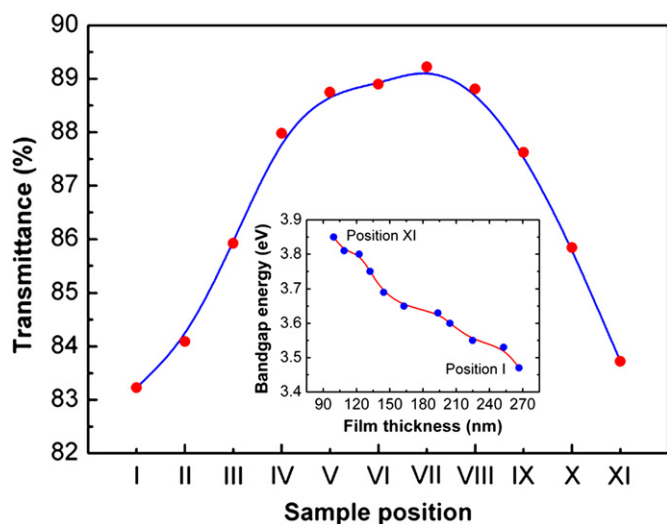


Fig. 4. Plot of average transmittance of WInZnO films as a function of the sample position. The inset shows the optical bandgap energy with the film thickness.

of film thickness at $W/(In+Zn+W)$ ratios of > 15.1 at%, while it may be in competition with each other at $W/(In+Zn+W)$ ratios of 8.6 – 15.1 at%. The inset in Fig. 4 shows the optical bandgap energy with different film thickness. Optical bandgap energies of the WInZnO films were found by plotting $(\alpha h\nu)^2$ vs. $h\nu$ and extrapolating to the energy axis. The optical bandgap energy increased gradually with reduction in film thickness as the sample position became close to W target (Position XI). According to the Burstein–Moss effect [15], the increase of the Fermi level in the conduction band leads to the broadening optical bandgap energy with increasing carrier concentration, but it cannot quantitatively describe the results shown in the inset of Fig. 4 because of reduction in carrier concentration. The detail electrical properties of WIZO films will be discussed. In our case, the change in optical bandgap energy seems to be the effect of the film thickness, which is expressed as

$$\Delta E_g \sim \frac{\hbar}{2m^*t^2} \quad (1)$$

where \hbar is Planck's constant divided by 2π , m^* is the effective carrier mass, and t is the film thickness [16]. Eq. (1) can generally explain the bandgap expansion with reduction of film thickness, i.e., the optical bandgap energy increases when the film thickness is reduced. The optical properties related to bandgap energy of

the WInZnO films have good correlation with the change in film thickness as shown in the inset of Fig. 4. A physical investigation using AFM was performed to evaluate the surface topography of the WInZnO composition spread films. The measured root-mean-square roughness value for all samples was about 0.25 nm (not shown here), which seems to be so smooth and contains few small grains, confirming the nearly amorphous nature of the WInZnO films. Thus, W incorporation did not influence the surface morphology of the amorphous matrix.

Fig. 5 shows the XRD patterns of the WInZnO composition spread films deposited on glass substrates at R.T using combinatorial rf magnetron co-sputtering system. The XRD patterns of the WInZnO films for sample positions between I and IV showed a halo peak with a mixture of the IZO phase and an amorphous phase around $2\theta=31^\circ$, and no sharp peaks appeared for all sample positions. Namely, all the XRD patterns of the films regardless of sample positions [$W/(In+Zn+W)$ ratio] exhibit the amorphous phase, indicating very small grain sizes and structurally disordered film. It seems that WO_3 was evenly embedded in the amorphous matrix ZnO-doped In_2O_3 .

Resistivity, carrier concentration, and Hall mobility of compositionally spread WInZnO films are shown in Fig. 6. Resistivity showed exponential curve as the sample position move toward position XI (WO_3 rich region), while the carrier concentration

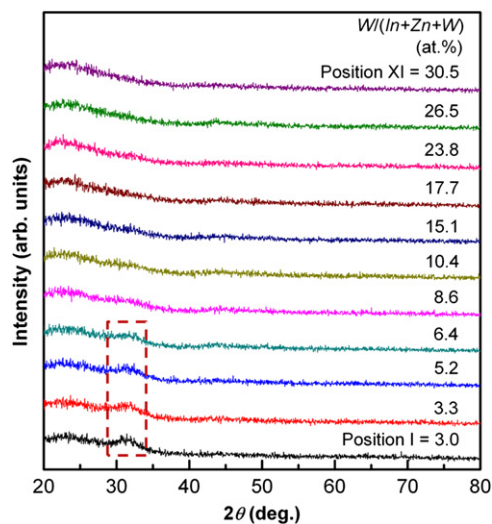


Fig. 5. XRD patterns of the compositionally spread WInZnO films deposited by combinatorial rf magnetron co-sputtering system.

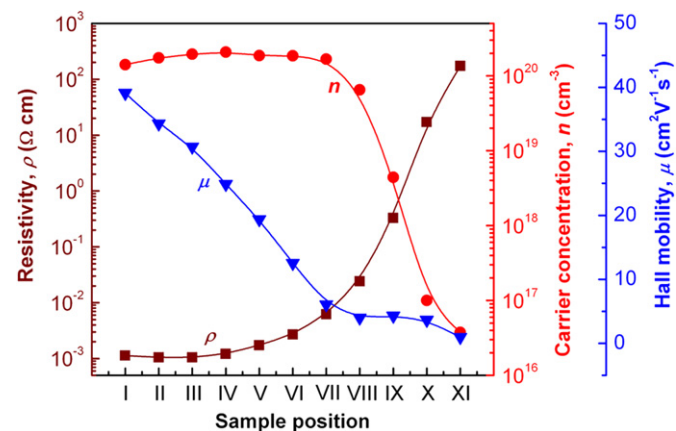


Fig. 6. Resistivity, carrier concentration, and Hall mobility of WInZnO films as a function of the sample position.

exhibited a reverse behavior and Hall mobility decreased gradually. This is apparent evidence that resistivity strongly depends on Hall mobility and carrier concentration. At the sample position I–VII [< 15.1 at% W/(In+Zn+W) ratio], resistivity was affected by Hall mobility rather than carrier concentration because the carrier concentration remained almost constant, attributing to the decrease in film thickness (see Fig. 3) and to the effect of a little incorporated W. The thinner film contains more structural defects and/or voids than thicker film. Since a larger scattering of carriers in the amorphous matrix, including very small grain sizes, could be existed in thinner film, the Hall mobility was limited by carrier trapping at localized state and ionized impurity scattering, resulting in the low mobility [17,18]. At the sample position VIII–XI [> 15.1 at% W/(In+Zn+W) ratio], the decrease in carrier concentration is major contributor to increase in resistivity, which is not a direct correlation of broadening optical bandgap energy as described in Fig. 4. These results can be explained by the fact that the carrier concentration is restricted by oxidation enhancement due to W incorporation as O binders, as discussed in Fig. 2. As a result, the WInZnO composition spread films having low carrier concentration ($< \sim 10^{18} \text{ cm}^{-3}$) deposited by combinatorial rf magnetron co-sputtering system is expected to expand further application fields to electronic devices including an active channel layer for oxide TFTs.

4. Conclusion

In summary, the WInZnO film prepared on glass substrate by combinatorial rf magnetron co-sputtering at R.T using the IZO and WO_3 targets was first introduced. A compositionally spread films accompanied by reduction in film thickness were made at once. The content of W and O elements increased gradually, as the sample position moved toward WO_3 target; namely, it is easy to control the chemical composition in the films by introducing the

combinatorial sputtering system. Furthermore, the bandgap energy increased with decreasing film thickness. All the films regardless of the sample position exhibited the amorphous phase. Incorporated W metal cations in the WInZnO film seemed to play a role in binding oxygen, because the electrical resistivity exponentially increased with decreasing carrier concentration.

References

- [1] Y. Vygranenko, K. Wang, A. Nathan, *Appl. Phys. Lett.* 91 (2007) 263508.
- [2] B.-Y. Oh, Y.-H. Kim, H.-J. Lee, B.-Y. Kim, H.-G. Park, J.-W. Han, G.-S. Heo, T.-W. Kim, K.-Y. Kim, D.-S. Seo, *Semicond. Sci. Technol.* 26 (2011) 085007.
- [3] D.-H. Cho, S. Yang, C. Byun, J. Shin, M.K. Ryu, S.-H.K. Park, C.-S. Hwang, S.M. Chung, W.-S. Cheong, S.M. Yoon, H.-Y. Chu, *Appl. Phys. Lett.* 93 (2008) 142111.
- [4] K. Nomura, H. Ohta, A. Takagi, T. Kamiya, M. Hirano, H. Hosono, *Nature* 432 (2004) 488.
- [5] N. Itagaki, T. Iwasaki, H. Kumomi, T. Den, K. Nomura, T. Kamiya, H. Hosono, *Phys. Status Solidi (a)* 205 (2008) 1915.
- [6] K.J. Saji, M.K. Jayaraj, K. Nomura, T. Kamiya, H. Hosono, *J. Electrochem. Soc.* 155 (2008) H390.
- [7] M.G. McDowell, R.J. Sanderson, I.G. Hill, *Appl. Phys. Lett.* 92 (2008) 013502.
- [8] H.S. Shin, G.H. Kim, W.H. Jeong, B.D. Ahn, H.J. Kim, *Jpn. J. Appl. Phys.* 49 (2010) 03CB01.
- [9] E. Chong, Y.S. Chun, S.Y. Lee, *Appl. Phys. Lett.* 97 (2010) 102102.
- [10] J.-S. Park, K. Kim, Y.-G. Park, Y.-G. Mo, H.D. Kim, J.K. Jeong, *Adv. Mater.* 21 (2009) 329.
- [11] W. Lim, E.A. Douglas, S.-H. Kim, D.P. Norton, S.J. Pearton, F. Ren, H. Shen, W.H. Chang, *Appl. Phys. Lett.* 95 (2009) 252103.
- [12] E. Chong, K.C. Jo, S.Y. Lee, *Appl. Phys. Lett.* 96 (2010) 152102.
- [13] G.-S. Heo, I.-G. Gim, J.-W. Park, K.-Y. Kim, T.-W. Kim, *J. Solid State Chem.* 182 (2009) 2937.
- [14] S.H. Jeong, J.H. Boo, *Thin Soild Films* 447 (2004) 105.
- [15] B.-Y. Oh, M.-C. Jeong, D.-S. Kim, W. Lee, J.-M. Myoung, *J. Cryst. Growth* 281 (2005) 475.
- [16] E.S.M. Goh, T.P. Chen, C.Q. Sun, Y.C. Liu, *J. Appl. Phys.* 107 (2010) 024305.
- [17] A.K. Saxena, S.P. Singh, R. Thangaraj, O.P. Agnihotri, *Thin Soild Films* 117 (1984) 95.
- [18] R. Martins, P. Barquinha, A. Pimentel, L. Pereira, E. Fortunato, *Phys. Status Solidi* 202 (2005) R95.